IEEE Photonics Journal
An IEEE Photonics Society Publication

Open Access

Multiband Ultrathin Polarization-Insensitive Terahertz Perfect Absorbers With Complementary Metamaterial and Resonator Based on High-Order Electric and Magnetic Resonances

Volume 10, Number 6, December 2018

Xiutao Huang
Conghui Lu
Cancan Rong
Zhaoyang Hu
Minghai Liu

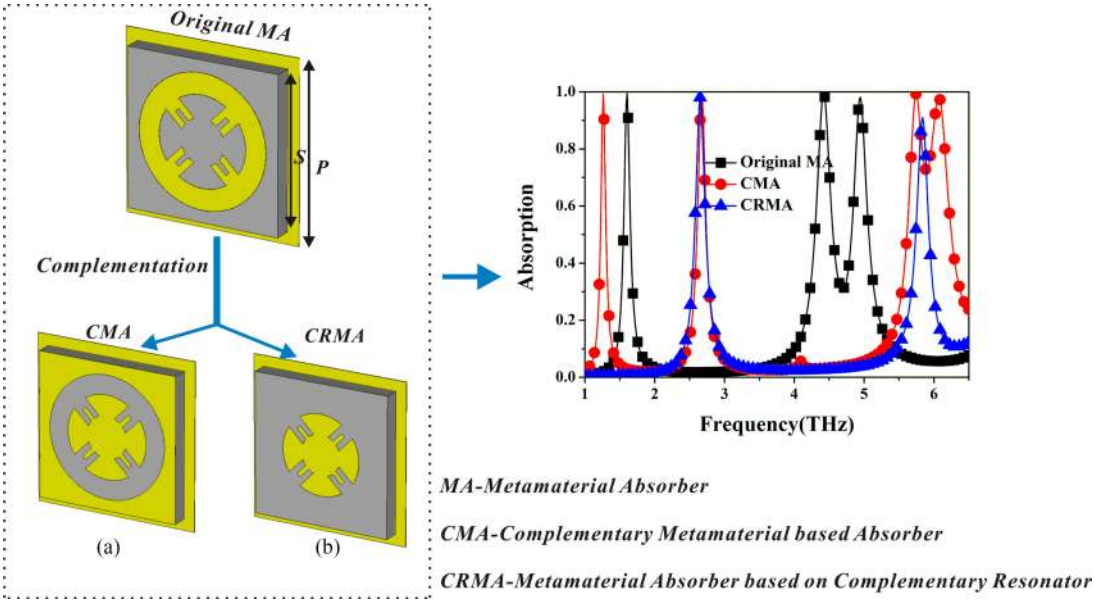

DOI: 10.1109/JPHOT.2018.2878455
1943-0655 © 2018 IEEE

Multiband Ultrathin Polarization-Insensitive Terahertz Perfect Absorbers With Complementary Metamaterial and Resonator Based on High-Order Electric and Magnetic Resonances

Xiutao Huang,[1] **Conghui Lu**,[2] **Cancan Rong**,[1] **Zhaoyang Hu**,[1] **and Minghai Liu** [1]

[1]State Key Laboratory of Advanced Electromagnetic Engineering and Technology, Huazhong University of Science and Technology, Wuhan 430074, China
[2]School of Physics, Huazhong University of Science and Technology, Wuhan 430074, China

DOI:10.1109/JPHOT.2018.2878455
1943-0655 © 2018 IEEE. Translations and content mining are permitted for academic research only. Personal use is also permitted, but republication/redistribution requires IEEE permission. See http://www.ieee.org/publications_standards/publications/rights/index.html for more information.

Manuscript received October 9, 2018; revised October 20, 2018; accepted October 24, 2018. Date of publication October 29, 2018; date of current version November 9, 2018. This work was supported in part by the National Key R&D Program of China under Grant 2018YFB0106300, in part by the Scientific Projects of State Grid Corporation of China under Grant 0231132705, in part by the National Natural Science Foundation of China under Grant 11575066, in part by the Graduates' Innovation Fund under Grant 5003131025, and in part by Huazhong University of Science and Technology. Corresponding author: Minghai Liu (E-mail mhliu@hust.edu.cn).

Abstract: Terahertz perfect metamaterial absorbers (PMA) based on higher order resonances have exhibited important applications in detecting, sensing, and imaging. However, most of them suffer from polarization and incident-angle dependence due to their asymmetrical structure. Here, we numerically investigate a kind of ultrathin triple-band PMA with polarization stability and wide angle of incidence. Numerical results reveal that three resonance peaks with nearly 100% absorptivity are obtained at 1.605, 4.425, and 4.946 THz under different polarization angles. It is interestingly found that the absorptance of two higher order resonances is inversely increased when the size of the middle dielectric spacer is smaller. The three resonance peaks in transverse electric and transverse magnetic modes nearly maintain fixed for oblique incidence up to 60°. Importantly, another four-band and dual-band perfect absorptions are easily achieved by a complementary method without doing iterative numerical simulation. The complementary metamaterial based absorber reaches more than 98% absorptance at four resonance frequencies. The metamaterial absorber based on complementary resonator also obtains two absorption peaks at 2.65 and 5.84 THz.

Index Terms: Complementary metamaterial, complementary resonator, Perfect metamaterial absorbers, polarization, wide angle.

1. Introduction

Terahertz (THz) devices have gained numerous interests in sensor [1], detector [2], [3], imaging [4]–[6]. An absorbing structure is usually one of important elements in these THz devices. Limited by the lack of natural absorbing materials in the terahertz gap, metamaterial absorbers (MAs), where the periodic elements are much smaller than the working wavelength of THz waves, have

been considered as an effective solution [7]–[9]. MAs are also used into selective thermal radiation, solar cells and stealth. Such kind of MAs are constructed by artificial meta-atoms. In the past years, various works on MAs have been proposed and demonstrated, such as single band [7], [8], dual band [9]–[11], triple band [12], multiband [13], [14], broadband [15], [16], polarization insensitive [16] and incident-angle insensitive operations. Single-band absorption can be easily obtained by the excitation of fundamental dipole resonance since the THz MA was firstly discovered [8]. In many cases, dual-bands or multiband absorptions have greater potential applications. Based on the overlapping of dipole resonance in the periodic elements, dual-band or multiband MAs have been reported by many researchers. For example, Ma *et al.* reported a dual band MA based on the combination of dipolar resonances of two nested squared rings [11]. Shen *et al.* demonstrated a triple-band MA by combining three concentric squared rings owing to excite three dipolar modes [12]. Hu *et al.* numerically designed a multiband THz MA by stacking two metal-dielectric layers [13]. Zhu *et al.* experimentally investigated an ultra-broadband THz MA using five-layer structure of metal-dielectric composite [15]. In the above discussion, multiband or broadband absorption can be obtained by utilizing differently-shaped and multilayer structure. Although these methods could be sufficient to improve the absorption performance of MA, they are heavily dependent on repetitive and time-consuming simulations to optimize different parameters of unit cell. In addition, it is impossible to continuously improve the absorption performance of MA by increasing the top patterns or metal-insulator layers.

To solve the above problems, the excitation of high-order resonance, which is often neglected, is a promising solution to quickly get multiband perfect absorption. Some research groups have reported the related works about the higher-order modes in the THz region. For example, Wu *et al.* discussed the absorption behaviors of a THz MA under different dielectric thicknesses and found two absorption modes in the process [17]. Wang *et al.* presented a dual-band THz MA made by a metallic strip, and the dual-band absorption was due to the excitation of the fundamental resonance and high-order mode [18]. Hu *et al.* discussed a multiband MA with U-shaped ring in the THz range, which originated from the multipolar resonance [19]. Shan *et al.* proposed a dual-band MA based on an asymmetric split ring, and the high-order resonance in asymmetric pattern was observed [20]. Cheng *et al.* numerically investigated a six-band PMA with cross-cave-patch structure which mainly arose from the multipolar resonance [21]. Yang *et al.* proposed a graphene based elliptic dielectric structure which can achieve broadband absorption in the THz range, and absorption mechanism came from multiple and continuous plasmon resonances [22]. However, there are few reports of absorption performance in a wide range of incident angle, and most of the above structures are asymmetric. Therefore, these MAs are polarization instability, which would limit their potential applications in many fields. In practice, it is desirable to simultaneously get the other MAs with perfect absorption due to the increasing demand of THz devices when one kind of MA is successfully designed.

Here, we propose an ultrathin polarization-insensitive wide-angle triple-band MA using only one resonator in the THz frequencies. It is composed of concave-strip ring and ground metallic film separated by spacer. Our simulation proves that a concave-strip ring can easily excite three perfect absorption peaks. Moreover, the absorption intensity of two high-order resonances is slightly stronger by decreasing the size of the middle spacer. Electric field (E_z) distributions of two metallic layers in the MA are employed to analyze the physical mechanism of perfect absorption. We demonstrate that the simple structure exhibits better absorption stability for wide incidence angles. Especially, under TE mode, the absorptivities of three resonance peaks all keep stable even up to 60°. To further extend kinds of MA, we quickly get two other MAs with high absorption by complementary strategy. Their physical origins are also investigated. We conclude that these MAs may develop many potential applications in sensor, detector and imaging.

2. Metamaterial Structure and Simulation Method

The MA of 6 × 6 arrays working at THz gap is depicted in Fig. 1(a). It consists of three layers from top to bottom, which are periodic concave-strip ring (CSR), a dielectric substrate and a continuous

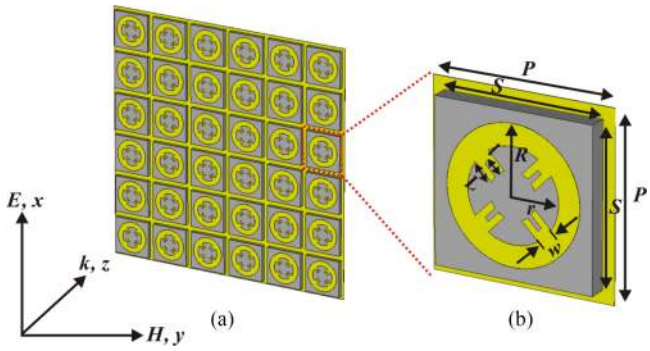

Fig. 1. (a) Schematic of the designed MA. (b) the geometrical structure of its unit cell.

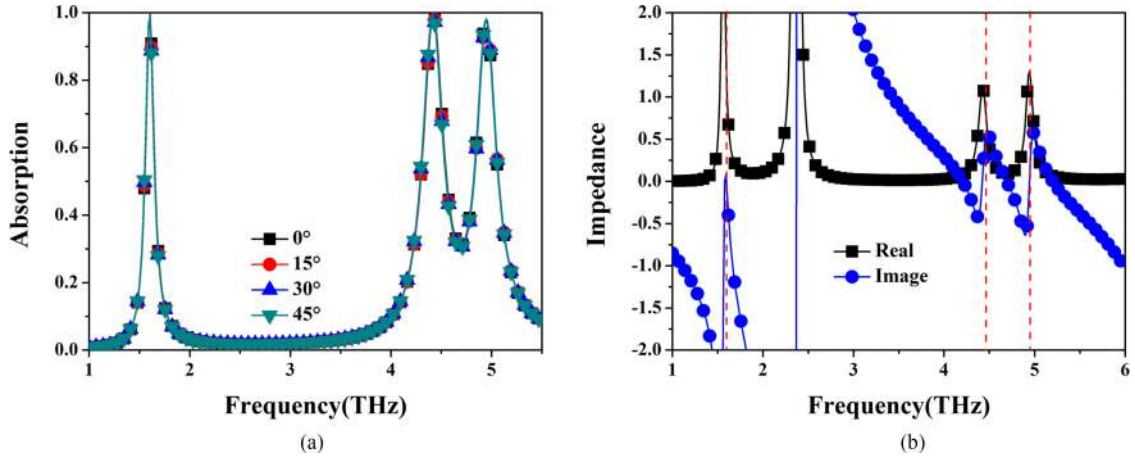

Fig. 2. (a) Dependence of simulated absorptance on different polarization angles, (b) normalized effective impedance.

metallic film. So, the periodic structure is typically a metal-insulator-metal (MIM) cavity, as shown in Fig. 1(b). When the electromagnetic (EM) waves work into the MIM cavity, they can be absorbed by optimizing geometry of unit cell. At first, initial guesses of all parameters in Fig. 1(b) are used to simulate unit cell. At second, we adjust several parameters to get the better absorption performance. Next, the values of l and L are mainly optimized to keep absorption stability under oblique incidence. The final geometrical parameters are $r = 7.5\ \mu$m, $R = 11\ \mu$m, $l = 2.4\ \mu$m, $L = 3.7\ \mu$m, and $w = 3\ \mu$m. Different from the previous THz MAs, the periodic length ($S = 26\ \mu$m) of dielectric layer is not equal to that ($P = 30\ \mu$m) of bottom metallic film in this MA. Here, the periodic length is still smaller than the resonance wavelength, as shown in Fig. 2. The dielectric layer (t) of 3 μm thickness is selected as GaAs substrate with a relative permittivity ($\varepsilon = 12.9 + 0.0774$i) [10] and two metallic layers is made up of gold with the conductivity of 4.56×10^7 S/m. Above geometric parameters are optimized by CST MICROWAVE STUDIO. Unit-cell boundary conditions are set along x and y directions and open boundary condition is used in z direction. Thus, the S parameters and 3D-electromagnetic (EM) characteristics of unit cell can be obtained from simulation results. Since the bottom metallic film eliminates transmission ($T(w)$), the absorption ratio ($A(w) = 1-R(w)$) of MA is completely determined by the reflectivity ($R(w)$). And, $R(w)$ depends on the effective impedance ($z(w) = \sqrt{\mu(w)/\varepsilon(w)}$). When $Z(w)$ is equal to 1 by tuning geometric parameters of the CSR, the proposed MA can realize perfect absorption.

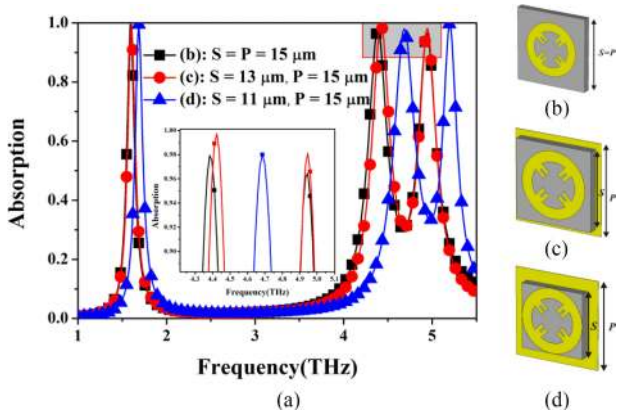

Fig. 3. (a) Simulated absorptance for different sizes of the middle dielectric substrate. (b)–(d) Perspective views of three unit cells with different dielectric lengths. Inset illustrates the enlarged photo of high-order modes.

3. Results and Discussions

The absorption properties of MA are mainly determined by the interaction of the top subwavelength pattern with the incident EM waves. In general, a resonant pattern can only get single absorption band. Owing to the rotational symmetry of the proposed structure, absorption results of both TE and TM normal incidence are consistent. In this work, Fig. 2(a) displays three absorption peaks induced by single CSR resonator under different polarization angles of TE normal incidence. The absorptivities of three resonance peaks are 99.4%, 99.6% and 98.2% at 1.605 THz, 4.425 THz and 4.946 THz, respectively. It is noted that the whole thickness of triple-band MA is 3.11 μm, which is only λ/60, λ/21.8 and λ/19.5 (λ is the resonance wavelength). Thus, the ultrathin MA achieves perfect absorption at different peaks. Their full width at half maximum (FWHM) is 0.1 THz, 0.24 THz, 0.25 THz under three resonant frequencies, respectively. The corresponding quality factor (Q = f/FWHM, where *f* is the resonance frequency) is 16.05, 18.44, 19.78. Especially, it is polarization-insensitive under normal incidence due to its symmetrical geometry. So, the designed perfect absorber can be used into THz detector. The advantage is that a single detector can respond to three-band thermal radiation.

To better analyze absorption phenomenon, relative wave impedance of the designed MA can be retrieved from *S* parameters [23]

$$Z(w) = \sqrt{\frac{(1 + S_{11}(w))^2 - S_{21}{}^2(w)}{(1 - S_{11}(w))^2 - S_{21}{}^2(w)}} \tag{1}$$

The result is shown in Fig. 2(b). Their real and imaginary parts are (0.98, −0.15), (1.07, 0.02) and (1.3, 0.07) at three resonance frequencies, respectively. It is clear that Re(Z) is near unity and Im(Z) is minimized, resulting in zero reflection. So, there exist the good impedance matching between our proposed structures and free space, which provides three near-unity absorptances.

In the previous papers, most researchers pay attention to the impact of CSR parameters and substrate thickness on the absorption characteristics. The dependence of the absorptance on the size of the middle insulator is rarely discussed. Although it is difficult to tune the size of the dielectric layer compared to other parameters so far in practice, the relationship between its sizes and absorption performance should be theoretically understood. In future work, we hope to make a sample by the advanced technology. When the periodic length of the middle insulator is equal to that of bottom metallic plane in Fig. 3(b), the proposed MA appears three high absorptivities of 99.4%, 97.9% and 96.4% at 1.605 THz, 4.38 THz and 4.946 THz in Fig. 3(a). Obviously, compared with the case of S = 13 μm in Fig. 3(c), the resonance frequencies of the first and third modes (f_1 and f_3) remain fixed while the second resonance peak slightly shifts to lower frequency.

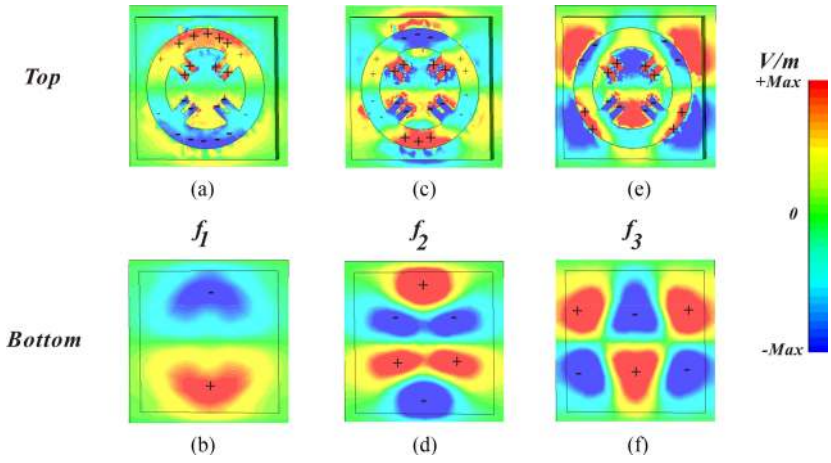

Fig. 4. The z-component electric field distributions (E_z) of top pattern in the MA: (a) 1.605 THz, (c) 4.425 THz and (e) 4.946 THz. The electric field (E_z) of bottom metallic plane: (b) 1.605 THz, (d) 4.425 THz and (f) 4.946 THz.

However, the absorptivities of high-order modes (f_2 and f_3) slightly drop. In other words, although the used material is decreased, the absorption performance of two high-order resonance peaks is interestingly improved. As the size further decreases, as shown in Fig. 3(d), three absorption peaks experience blue-shifted while the corresponding absorptivities still maintain more than 96%. Therefore, the designed MA can achieve better absorptivity as well as saves some materials in the case of $S = 13$ μm and $P = 15$ μm. Based on the equivalent circuit theory, the inductance (L) and capacitance (C) determine the resonance frequency ($f = 1/2\pi\sqrt{L\,C}$) [24]. The capacitance C can be simply defined by the formula of parallel plate capacitor $C = \varepsilon_r\varepsilon_0 s_0/(4t)$, where ε_r is relative permittivity of the middle dielectric layer and s_0 is the equivalent area of upper metallic pattern. When the dielectric layer becomes smaller, the effective capacitance decreases, resulting in blueshift of the absorption peak.

The electric field (E_z) is employed to analyze the original mechanism of three perfect absorptions in detail. Fig. 4 illustrates the z-component distributions of electric field with different resonant modes on the top pattern and bottom plane. In Fig. 4(a) and (b), a pair of induced charges are gathered on both parts of MA along E direction. It indicates that electric dipole is excited on the top and ground metal, respectively. In Fig. 4(a), gap surface plasmons on the middle dielectric layer are excited [25], [26] and are opposite phase with dipolar CSR mode. Moreover, the phase of dipolar resonance on the bottom metal is opposite to that of dipolar CSR mode. So, the strong coupling between them can lead to a magnetic resonance. Both electric and magnetic dipole resonances give rise to perfect absorption at 1.605 THz. In Fig. 4(c) and (d), we can observe two pairs of induced charges on either side [27]. The results manifest that electric quadrupoles on the CSR pattern and metallic plane are simultaneously generated, and they are anti-phase with each other, which result in two-harmonic magnetic resonance [28]. Thus, the perfect absorption at 4.425 THz comes from the generation of high-order resonances (electric quadrupolar and two-harmonic magnetic mode). In Fig. 4(e) and (f), three dipolar pairs are generated by the accumulation of induced positive-negative charges on both sides of top and bottom metallic plane. Obviously, the electric hexapoles at the top and bottom metal are observed, and they are opposed phase with each other. So, three-harmonic magnetic resonance is formed owing to the strong interaction of these hexapolar modes [28]. Therefore, the high absorption at 4.946 THz is due to generate the higher-order EM resonances. In summary, both fundamental and high-order EM resonances support the high absorption of the designed MA.

Based on the above discussion of electric field, the concave strip in CSR pattern plays an important role in triple-band absorption. Thus, we numerically analyze the influence of concave-strip inner and outer lengths (l and L) on absorptivity. In Fig. 5(a), the CSR resonator still maintains

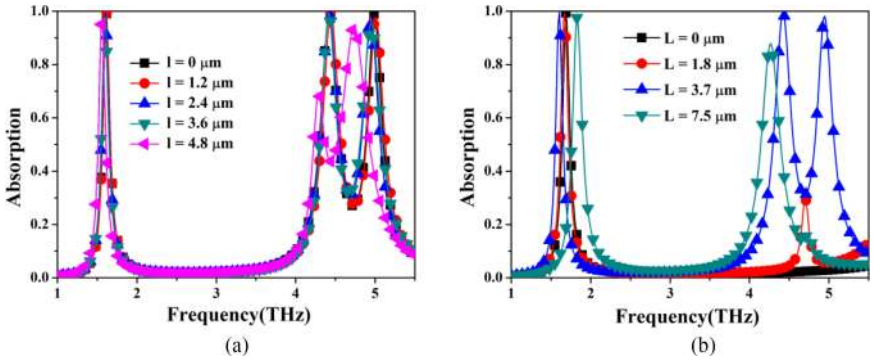

Fig. 5. Simulated absorptance with (a) different concave-strip inner length (l) and (b) different concave-strip outer length (L).

high absorption and the three resonance peaks occur slightly red-shifted as the inner length (l) increases. It is noted that the absorptivity of high-order mode (f_2) significantly reduces when the value of inner length is equal to 4.8 μm. The increase of equivalent capacitance in the resonator causes the slight decrease of three resonant frequencies. In Fig. 5(b), the change of outer length (L) has a larger impact on the absorption performance of the proposed MA. When the resonator shows the ring structure ($L = 0$ μm), single peak can be obtained. Dual peaks or triple peaks can be observed as the concave strip appears. The reason is that the ring resonator with concave strip not only generate dipole resonance but also excite higher-order modes, as shown in Fig. 4. Therefore, the outer length (L) of concave strip controls higher order modes.

In the case of normal incidence, triple-band perfect absorption has been discussed in the above section. In the practical work, it is preferable to maintain high absorption under oblique angle of incidence. Thus, the absorption characteristics of the designed MA for wide angle of incidence are given in Fig. 6. For transverse electric (TE) mode in Fig. 6(a) and (b), the three absorption peaks hardly move as the incident angle changes. Especially, their absorptivities are still over 80% even when increasing to 60°. For transverse magnetic (TM) mode in Fig. 6(c) and (d), three resonant frequencies almost maintain stable and their absorptivities are above 88% even up to 60°. It is found that additional peaks are generated for both TE and TM mode. The reason is that there may exist the equal decay between the EM radiation and material absorption at an incident angle [22]. That is to say, this phenomenon may be due to the special ratios between geometrical structure of the CSR and the wavelength of additional peaks [29], [30].

To further highlight the angle-insensitive advantage of the designed PMA, we compare with the previous literatures about high-order modes based MA [21], [22], [31]–[33], as depicted in Table 1. Although multiband absorption based on the fundamental and higher-order modes has been demonstrated by many researchers, the absorption performance under wide angle of incidence is hardly discussed. Moreover, most of the THz MAs in the previous reports are obviously sensitive to polarization due to the asymmetric structure itself. In our works, the designed structure not only reaches triple-band absorption for wide angular range but also appears polarization-insensitive performance. And, its thickness is thinner by comparisons. It is believed that the good merits of the proposed structure will contribute to the development of multiband MA.

4. Two Kinds of Complementary MAs

It is well known that numerical optimization is common approach to get certain MA so far. As such, we need spend a lot of time repetitively optimizing the simulation models again when another MA is required. Hence, we take advantage of a complementary strategy to easily obtain other MAs. Of course, we agree that the proposed solution would not fundamentally solve the designed way. However, it can effectively save the consuming time. When the square metal which is equal to the

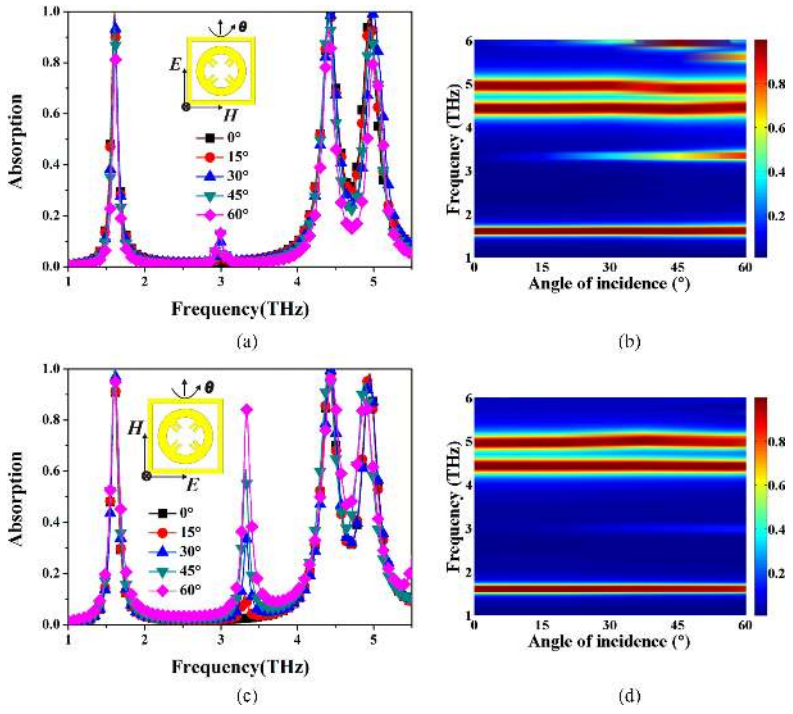

Fig. 6. Simulated absorptivity with different angles of incidence: (a) and (b) TE mode, (c) and (d) TM mode.

TABLE 1
Comparison With Our Work and Previous Reports

References	NRP	Thickness (μm)	MA at 0°		A at 60°		Polarization insensitivity
			TE	TM	TE	TM	
21	6	3.8(0.04λ)	98.7%	98.7%	No discussion	No discussion	Yes
22	broadband	28(0.28λ)	No discussion	99%	No discussion	80%	No
31	3	0.44(0.13λ)	90%	90%	No discussion	No discussion	No
32	4	11(0.15λ)	99%	96%	No discussion	No discussion	No
33	3	0.3(0.21λ)	99.5%	99.5%	No discussion	No discussion	Yes
This work	3	3.11(0.05λ)	99.6%	99.6%	80%	88%	Yes

MA, Maximal Absorptivity; NRP, Number of Resonant Peaks; λ, resonance wavelength of highest peak

size of the middle substrate subtracts the original pattern, another absorber is simply obtained, which is defined as complementary metamaterial based absorber (CMA) in Fig. 7(a). When the rounded metal which is equal to the size of the top resonator subtracts the original pattern, another MA based on complementary resonator (CRMA) is easily designed in Fig. 7(b). The absorption ratio of two MAs is shown in Fig. 8.

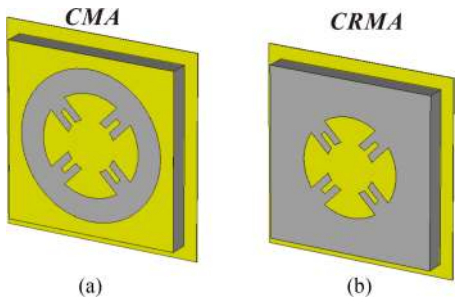

Fig. 7. (a) Schematic of complementary metamaterial based absorber (CMA). (b) Schematic of complementary resonator based metamaterial absorber (CRMA).

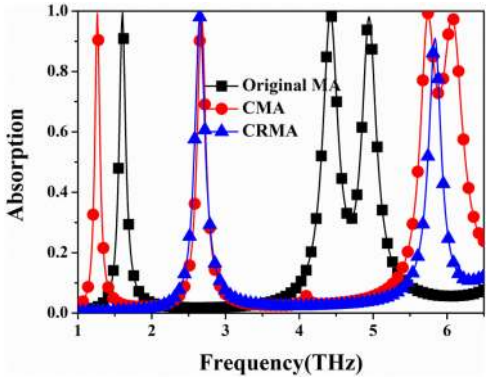

Fig. 8. Performance comparison of original MA, CMA and CRMA.

It can be seen that the CMA appears four distinct resonance peaks with the absorptance of 99.2%, 98.8%, 99.3%, and 98.1% at 1.26 THz, 2.66 THz, 5.74 THz, and 6.06 THz, respectively. A wide absorption band with the absorptivity of higher than 72.5% is formed from 5.66 THz to 6.18 THz. The number of its absorption peaks is one more than those of original MA. The CRMA excites two absorption peaks with the absorptivities of 98% and 91% located at 2.65 THz and 5.84 THz which are one less than the number of resonance peaks of original MA. It is carefully observed that the second peak of CMA is almost identical to the first peak of CRMA.

To explain the physical origin of CMA and CRMA, we give the electric field (E_z) distributions at distinct absorption frequencies. In Fig. 9(a) and (b), a pair of charges are confined around the upper and lower region of the top like-square structure and bottom metal, and the phase of outer patch is the opposite of ground plane. So, both electric dipole mode and a magnetic resonance lead to high absorption at 1.26 THz. As depicted in Fig. 9(c) and (d), the upper and lower edges of like-sector structure and the same parts of grounded metal appear the accumulation of negative-positive/positive-negative charges. It is found that the electric field (E_z) distributions of CRMA in Fig. 9(i) and (g) are nearly the same as the case of CMA in Fig. 9(c) and (d). Thus, the similar absorption characteristics of CMA and CRMA around 2.65 THz are caused by the excitation of dipole like-sector mode and a magnetic resonance.

For the resonance peak of 5.74 THz, the positive-negative charges are obviously concentrated at air-metal and dielectric-ground interfaces, as depicted in Fig. 9(e) and (f). Electric quadrupole like-square mode and dipole like-sector mode in Fig. 9(e) are generated, which are anti-phase with electric octopole mode in Fig. 9(f). So, the EM coupling between them forms four-harmonic magnetic resonance. For the resonance peak of 6.06 THz, Electric quadrupole like-square mode is anti-phase with the electric hexapole like-sector mode in Fig. 9(g), and the strong coupling between the top and bottom metal can excite two-harmonic magnetic resonance. The EM phenomenon in

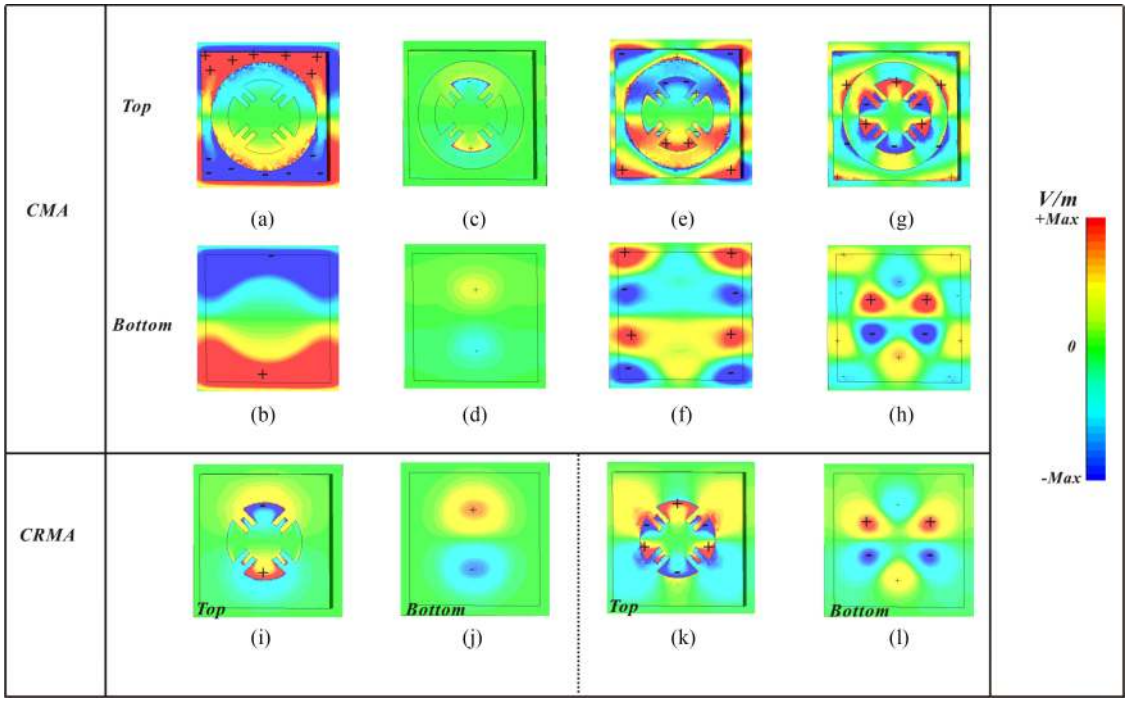

Fig. 9. Electric field (E_z) distributions of CMA at the top plane: (a) 1.26 THz, (c) 2.66 THz, (e) 5.74 THz, and (g) 6.06 THz; at the bottom metal: (b) 1.26 THz, (d) 2.66 THz, (f) 5.74 THz, and (h) 6.06 THz. Electric field distribution (E_z) of CRMA at the top plane: (i) 2.65 THz and (k) 5.84 THz; at the ground plane: (g) 2.65 THz and (l) 5.84 THz.

Fig. 9(k) and (l) is similar to that in Fig. 9(g) and (h). Therefore, the high absorption of CRMA at 5.84 THz is due to inspire the electric quadrupole mode and two-harmonic magnetic resonance.

In Fig. 9(e), "$+-+-$" along vertical direction can be used to represent the direction of electric field. In Fig. 9(g), the electric field along vertical direction can be expressed as "$++-+--$". It implies that the plasmon hybridization between like-square and like-sector pattern leads to a wide absorption among the frequency range of 5.66–6.17 THz [34], [35]. In summary, four absorption bands of CMA are mainly due to the excitation of like-square dipole mode, like-sector dipole mode, and plasmon hybridization. Therefore, plasmon hybridization formed in CMA leads to the increase of absorption peaks compared to original MA.

5. Conclusions

To conclude, we have numerically demonstrated a ultrathin, single-pattern, triple-band PMA by utilizing the excitation of higher-order resonances. In particular, the triple-band PMA simultaneously appears the characteristics of polarization and wide-angle insensitivity for TE and TM modes. Moreover, it is interesting that the absorptivities of the second and third resonance peaks are slightly increased by the size reduction of the middle substrate. The electric field (E_z) distributions indicate that perfect absorption at 1.605 THz, 4.425 THz and 4.946 THz comes from the production of electric dipole mode and a magnetic resonance, electric quadrupole mode and two-harmonic magnetic resonance, electric hexapole mode and three-harmonic magnetic resonance, respectively. More importantly, we can quickly get another four-band and dual-band MA by complementary approach. The physical origin is detailedly analyzed by the z-component electric field distributions of top and bottom metallic plane. Meanwhile, the mentioned method can be extended to the other spectral bands.

References

[1] H. T. Chen, W. J. Padilla, J. M. Zide, A. C. Gossard, A. J. Taylor, and R. D. Averitt, "Active terahertz metamaterial devices," *Nature*, vol. 444, no. 7119, pp. 597–600, Nov. 2006.

[2] S. J. Park *et al.*, "Detection of microorganisms using terahertz metamaterials," *Sci. Rep.*, vol. 4, May 2014, Art. no. 4988.

[3] W. R. Zhu, F. J. Xiao, M. Kang, D. Sikdar, and M. Premaratne, "Tunable terahertz left-handed metamaterial based on multi-layer graphene-dielectric composite," *Appl. Phys. Lett.*, vol. 104, no. 5, Feb. 2014, Art. no. 051902.

[4] C. M. Watts *et al.*, "Terahertz compressive imaging with metamaterial spatial light modulators," *Nat. Photon.*, vol. 8, no. 8, pp. 605–609, Jun. 2014.

[5] N. I. Landy, C. M. Bingham, T. Tyler, N. Jokerst, D. R. Smith, and W. J. Padilla, "Design, theory, and measurement of a polarization-insensitive absorber for terahertz imaging," *Phys. Rev. B*, vol. 79, no. 12, Mar. 2009, Art. no. 125104.

[6] I. Escorcia Carranza, J. P. Grant, J. Gough, and D. Cumming, "Terahertz metamaterial absorbers implemented in CMOS technology for imaging applications: Scaling to large format focal plane arrays," *IEEE J. Sel. Topics Quantum Electron.*, vol. 23, no. 4, Jul./Aug. 2017, Art. no. 4700508.

[7] H. Tao *et al.*, "Highly flexible wide angle of incidence terahertz metamaterial absorber: Design, fabrication, and characterization," *Phys. Rev. B*, vol. 78, no. 24, Dec. 2008, Art. no. 241103.

[8] H. Tao, N. I. Landy, C. M. Bingham, X. Zhang, R. D. Averitt, and W. J. Padilla, "A metamaterial absorber for the terahertz regime: Design, fabrication and characterization," *Opt. Express*, vol. 16, no. 10, pp. 7181–7188, May 2008.

[9] H. Tao *et al.*, "A dual band terahertz metamaterial absorber," *J. Phys. D, Appl. Phys.*, vol. 43, no. 22, May 2010, Art. no. 225102.

[10] Q. Y. Wen, H. W. Zhang, Y. S. Xie, Q. H. Yang, and Y. L. Liu, "Dual band terahertz metamaterial absorber: Design, fabrication, and characterization," *Appl. Phys. Lett.*, vol. 95, no. 24, Dec. 2009, Art. no. 241111.

[11] Y. Ma, Q. Chen, J. Grant, S. C. Saha, A. Khalid, and D. R. Cumming, "A terahertz polarization insensitive dual band metamaterial absorber," *Opt. Lett.*, vol. 36, no. 6, pp. 945–947, Mar. 2011.

[12] X. P. Shen *et al.*, "Triple-band terahertz metamaterial absorber: Design, experiment, and physical interpretation," *Appl. Phys. Lett.*, vol. 101, no. 15, Oct. 2012, Art. no. 154102.

[13] F. R. Hu *et al.*, "Design of a polarization insensitive multiband terahertz metamaterial absorber," *J. Phys. D: Appl. Phys.*, vol. 46, no. 19, Apr. 2013, Art. no. 195103.

[14] R. Yahiaoui, J. P. Guillet, F. De Miollis, and P. Mounaix, "Ultra-flexible multiband terahertz metamaterial absorber for conformal geometry applications," *Opt. Lett.*, vol. 38, no. 23, pp. 4988–4990, Dec. 2013.

[15] J. F. Zhu, Z. F. Ma, W. J. Sun, F. Ding, Q. He, L. Zhou, and Y. G. Ma, "Ultra-broadband terahertz metamaterial absorber," *Appl. Phys. Lett.*, vol. 105, no. 2, Jul. 2014, Art. no. 021102.

[16] J. Grant, Y. Ma, S. Saha, A. Khalid, and D. R. Cumming, "Polarization insensitive, broadband terahertz metamaterial absorber," *Opt. Lett.*, vol. 36, no. 17, pp. 3476–3478, Sep. 2011.

[17] K. M. Wu, Y. J. Huang, T. L. Wanghuang, W. J. Chen, and G. J. Wen, "Numerical and theoretical analysis on the absorption properties of metasurface-based terahertz absorbers with different thicknesses," *Appl. Opt.*, vol. 54, no. 2, pp. 299–305, Jan. 2015.

[18] B. X. Wang, X. Zhai, G. Z. Wang, W. Q. Huang, and L. L. Wang, "A novel dual-band terahertz metamaterial absorber for a sensor application," *J. Appl. Phys.*, vol. 117, no. 1, Jan. 2015, Art. no. 014504.

[19] D. Hu, H. Y. Wang, and Q. F. Zhu, "Design of six-band terahertz perfect absorber using a simple U-shaped closed-ring resonator, " *IEEE Photon. J.*, vol. 8, no. 2, Mar. 2016, Art. no. 5500608.

[20] Y. Shan, L. Chen, C. Shi, Z. X. Cheng, X. F. Zang, B. Q. Xu, and Y. M. Zhu, "Ultrathin flexible dual band terahertz absorber," *Opt. Commun.*, vol. 350, pp. 63–70, Sep. 2015.

[21] Y. Z. Cheng, M. L. Huang, H. R. Chen, Z. Z. Guo, X. S. Mao, and R. Z. Gong, "Ultrathin six-band polarization-insensitive perfect metamaterial absorber based on a cross-cave patch resonator for terahertz waves," *Materials*, vol. 10, no. 6, May 2017, Art. no. 591.

[22] J. W. Yang *et al.*, "Broadband terahertz absorber based on multi-band continuous plasmon resonances in geometrically gradient dielectric-loaded graphene plasmon structure," *Sci. Rep.*, vol. 8, no. 1, Feb. 2018, Art. no. 3239.

[23] D. R. Smith, D. C. Vier, Th. Koschny, and C. M. Soukoulis, "Electromagnetic parameter retrieval from inhomogeneous metamaterials," *Phys. Rev. E*, vol. 71, no. 3, Mar. 2005, Art. no. 036617.

[24] J. F. Zhou, L. Zhang, G. Tuttle, T. Koschny, and C. M. Soukoulis, "Negative index materials using simple short wire pairs," *Phys. Rev. B*, vol. 73, no. 4, Jan. 2006, Art. no. 041101.

[25] X. T. Huang, C. H. Lu, C. C. Rong, S. M. Wang, and M. H. Liu, "Wide angle of incidence-insensitive polarization-independent thz metamaterial absorber for both te and tm mode based on plasmon hybridizations," *Materials*, vol. 11, no. 5, Apr. 2018, Art. no. 671.

[26] A. Chakrabarty, F. Wang, F. Minkowski, K. Sun, and Q. H. Wei, "Cavity modes and their excitations in elliptical plasmonic patch nanoantennas," *Opt. Express*, vol. 20, no. 11, pp. 11615–11624, May 2012.

[27] X. Chen, W. H. Fan, and C. Song, "Multiple plasmonic resonance excitations on graphene metamaterials for ultrasensitive terahertz sensing," *Carbon*, vol. 133, pp. 416–422, Jul. 2018.

[28] N. V. Dung *et al.*, "Perfect and broad absorption by the active control of electric resonance in metamaterial," *J. Opt.*, vol. 17, no. 4, Mar. 2015, Art. no. 045105.

[29] F. Costa, S. Genovesi, A. Monorchio, and G. Manara, "A circuit-based model for the interpretation of perfect metamaterial absorbers," *IEEE Trans. Antennas Propag.*, vol. 61, no. 3, pp. 1201–1209, Mar. 2013.

[30] M. D. Astorino, F. Frezza, and N. Tedeschi, "Ultra-thin narrow-band, complementary narrow-band, and dual-band metamaterial absorbers for applications in the THz regime," *J. Appl. Phys.*, vol. 121, no. 6, Feb. 2017, Art. no. 063103.

[31] G. Dayal and S. A. Ramakrishna, "Multipolar localized resonances for multi-band metamaterial perfect absorbers," *J. Opt.*, vol. 16, no. 9, Sep. 2014, Art. no. 094016.

[32] B. X. Wang, "Quad-band terahertz metamaterial absorber based on the combining of the dipole and quadrupole resonances of two SRRs," *IEEE J. Sel. Topics Quantum Electron.*, vol. 23, no. 4, Mar. 2017, Art. no. 4700107.
[33] L. Zhao, H. Liu, Z. H. He, and S. K. Dong, "Theoretical design of twelve-band infrared metamaterial perfect absorber by combining the dipole, quadrupole, and octopole plasmon resonance modes of four different ring-strip resonators," *Opt. Express*, vol. 26, no. 10, pp. 12838–12851, May 2018.
[34] E. Prodan, C. Radloff, N. J. Halas, and P. Nordlander, "A hybridization model for the plasmon response of complex nanostructures," *Science*, vol. 302, no. 5644, pp. 419–422, Oct. 2003.
[35] N. L. Mou, S. L. Sun, H. X. Dong, S. H. Dong, Q. He, L. Zhou, and L. Zhang, "Hybridization-induced broadband terahertz wave absorption with graphene metasurfaces," *Opt. Express*, vol. 26, no. 9, pp. 11728–11736, Apr. 2018.